Journal of Catalysis 282 (2011) 289–298

Contents lists available at ScienceDirect

Journal of Catalysis

journal homepage: www.elsevier.com/locate/jcat

A mechanistic study on soot oxidation over CeO_2–Ag catalyst with 'rice-ball' morphology

Kiyoshi Yamazaki *, Tomoyuki Kayama, Fei Dong, Hirofumi Shinjoh

Toyota Central R&D Laboratories Inc., Nagakute, Aichi 480-1192, Japan

ARTICLE INFO

Article history:
Received 21 January 2011
Revised 30 May 2011
Accepted 2 July 2011
Available online 10 August 2011

Keywords:
Soot oxidation
Silver
Ceria
Morphology
Reaction mechanism
Diesel emission control

ABSTRACT

A CeO_2–Ag catalyst with a 'rice-ball' morphology, consisting of Ag particles in the center surrounded by fine CeO_2 particles, exhibits exceptional catalytic performance for soot oxidation by O_2 below 300 °C. The reaction mechanism over this catalyst was studied by O_2 temperature-programmed desorption (O_2-TPD), $^{18}O/^{16}O$ isotopic exchange (IE) reaction, and electron spin resonance (ESR) techniques. It is speculated that adsorbed oxygen species on the Ag surface migrate to the CeO_2 surface via the Ag/CeO_2 interface to form O_n^{x-} species (at least partly O_2^-) and further migrate onto the soot particles. Due to morphological compatibility of the moderately large Ag particles (ca. 30–40 nm) and the extremely large interfacial area with the CeO_2 particles, the formation and migration rates of the oxygen species on the CeO_2–Ag catalyst are efficiently promoted, resulting in its distinguished catalytic performance and relative insensitivity to the contact mode of the soot–catalyst mixture.

1. Introduction

In recent years, diesel-powered vehicles have increased their market share in the world, due to lower fuel consumption, higher durability and reliability in comparison with gasoline-powered vehicles. Diesel engines are expected to play a positive role in the prevention of global warming by increased fuel efficiency and thus lower CO_2 emission than gasoline engines. However, there is a strong demand for the abatement of nitrogen oxide (NO_x; NO + NO_2) and particulate matter (PM; mainly 'soot') from diesel engines, which can give rise to serious environmental and health problems. The severity of new emission regulations requires solutions based on suitable after-treatment technologies, as well as technical improvements to the engines. The most effective and widely applied after-treatment technology for PM control is based on the diesel particulate filter (DPF). Soot trapped in a DPF must be periodically removed by combustion, due to unacceptable back pressure levels in the gas exhaust line. The direct oxidation of soot over the un-catalyzed DPF requires high temperatures around 600 °C and is generally carried out by injecting diesel fuel into the exhaust. This strategy incurs additional fuel consumption, requires a complex means of control, and can create significant thermal stress for the DPF and the other after-treatment devices (i.e., the de-NO_x catalysts).

A catalyzed diesel particulate filter (C-DPF) is regarded as the most promising solution to reduce PM emissions from diesel engines, where the soot is trapped and oxidized with a catalyst at lower temperature. However, large soot particles are immobile and barely penetrate into the catalyst micropores or mesopores, and thus, catalytic soot oxidation is quite slow [1,2]. The major problem with the C-DPF is the poor contact between the external catalyst surface and the soot particles. To overcome this problem, many catalysts and technologies based on different principles have been proposed. Using gas-phase NO_2 in the application of so-called continuously regeneration trap (CRT) technology causes a decrease in the soot oxidation temperature [3]. NO_2 is generated from the oxidation of NO over a platinum catalyst and functions as a mobile species for soot oxidation by creating catalyst–soot contact; however, a new trend in diesel engines to decrease NO_x emission could impose significant restrictions on the application of CRT technology. Organometallic fuel additives, also known as fuel-borne catalysts (FBCs), lead to the formation of catalyst-doped soot during combustion in the engine, which lowers the soot oxidation temperature in the DPF [4,5]; however, the continuous consumption of FBCs and the accumulation of metal oxide as an ash inside the DPF restrict their application strongly. A large number of molten salt catalysts, which can wet the soot surface as a mobile catalyst and therefore decrease the soot oxidation temperature, have been studied in recent years; the formulations are based on the addition of potassium or cesium to transition metal (such as Cu, V, Mo, Co, or Fe) oxides [6–10], combinations of Co, K/MgO or Ba, K/CeO_2 [11–13], and perovskites such as $LaCrO_3$ and $La_{0.9}K_{0.1}Cr_{0.9}O_3$ [14].

* Corresponding author.
E-mail address: e0936@mosk.tytlabs.co.jp (K. Yamazaki).

0021-9517/$ - see front matter © 2011 Elsevier Inc. All rights reserved.
doi:10.1016/j.jcat.2011.07.001

However, these catalysts have drawbacks in some practical applications that are related to either thermal degradation or selective leaching in condensed water during the soot oxidation process [15].

Recently, many researchers have reported that CeO_2-based oxides have good activity for soot oxidation at lower temperature [16–23]. Aneggi et al. studied the effect of Ag addition on the soot oxidation activity of various metal oxides [24]; the addition of Ag to ZrO_2 and Al_2O_3 resulted in very active catalysts, while addition to CeO_2 had little benefit. On the other hand, Machida et al. and Shimizu et al. reported that Ag loading onto CeO_2 enhanced the catalytic activity for soot oxidation [25,26]. However, the design concept of these catalysts, i.e., morphology control based on the functions of Ag and CeO_2, has not been devoted to the problem of catalyst–soot particle contact. In addition, silver-supporting catalysts may suffer from performance degradation due to Ag sintering under oxidative conditions at temperatures around 400 °C [27].

Considering this background, we have developed an innovative CeO_2–Ag catalyst, which exhibits exceptional performance for soot oxidation with gaseous oxygen at temperatures below 300 °C [28]. This catalyst has a unique agglomeration morphology, as shown in Fig. 1, in which the scanning electron microscopy (SEM) image (a) shows that this catalyst consists of numerous spherical 'balls' with diameters of about 100 nm and the transmission electron microscopy (TEM) image of the cut plane of a single ball (b) shows that the center Ag metal is surrounded by fine CeO_2 particles. The morphology of this catalyst is schematically illustrated in Fig. 2, in which the unique agglomeration nanostructure is similar to a Japanese 'rice-ball', consisting of a center composed of Ag particles (rice-ball filling) surrounded by fine CeO_2 particles (grains of rice). This morphology was designed to increase the Ag/CeO_2 interface area per unit surface area of Ag particles and to inhibit Ag sintering, because thermally stable CeO_2 particles act as barriers to sintering. A CeO_2–Ag catalyst with such morphology was synthesized by a novel nanofabrication method based on precipitation between aqueous solutions of nitrates and ammonia [28].

In this study, temperature-programmed oxidation (TPO) over the soot/catalyst mixture under tight and loose contact modes was used to evaluate the catalytic performance. To reveal the different aspects involved in catalytic soot oxidation, oxygen temperature-programmed desorption (O_2-TPD), $^{18}O/^{16}O$ isotopic exchange (IE) reaction, and electron spin resonance (ESR) techniques were employed to characterize the active property of oxygen species, oxygen mobility or migration rates and identification of oxygen species, respectively. Through discussing these characterization results and correlating with their catalytic performances, we tried to elucidate the mechanism involved in catalytic soot oxidation, especially over the CeO_2–Ag catalyst with unique "rice-ball" morphology, which exhibits an overwhelmingly high catalytic performance among the prepared catalysts.

2. Experimental

2.1. Catalyst preparation

A CeO_2–Ag catalyst was synthesized by a coprecipitation-based method. One hundred and fifty milliliters aqueous solution of $AgNO_3$ (Toyo Chemical Industrial, 29.63 g) and $Ce(NO_3)_3{\cdot}6H_2O$ (Wako Pure Chemical Industries, 50.49 g) was added to a diluted ammonia solution (35.6 g of 25% ammonia solution, diluted by 100 mL of water) instantly (in less than a second) with a rotary stirrer (350 rpm) at room temperature. The mixture was stirred for 1 min, and the coprecipitate was heated uniformly by steam in an autoclave at 120 °C for 10 min. The gained coprecipitate was separated by centrifugation and calcined at 500 °C for 5 h in air. The Ag content of the obtained CeO_2–Ag catalyst was 39 wt.%. A more detailed description of the catalyst preparation is given elsewhere [28].

Ag(x)/CeO_2, Ag(x)+CeO_2, Ag(x)/Al_2O_3, and CeO_2 catalysts, where 'x' denotes the Ag content in wt.%, were used as reference catalysts. The CeO_2 catalyst was obtained by calcination of a commercial CeO_2 powder (Rhodia, BET surface area 150 m^2/g) at 600 °C for 50 h, with a BET surface area of 78 m^2/g. The Ag(x)/CeO_2 catalysts were prepared by impregnation of the CeO_2 catalyst with aqueous $AgNO_3$ solution and calcination at 500 °C for 5 h in air. The Ag(x)+CeO_2 catalysts were prepared by physical mixing of the CeO_2 catalyst and a commercial Ag powder (Nisshin Engineering, BET surface area 9 m^2/g) with a magnetically driven mortar for 20 min followed by calcination at 300 °C for 5 h in air. The Ag(x)/Al_2O_3 catalysts were prepared by impregnation of a commercial Al_2O_3 powder (Showa Denko, UA-5205 with BET surface area 25 m^2/g) with aqueous $AgNO_3$ solution followed by calcination at 500 °C for 5 h in air.

2.2. Catalytic performance evaluation

The catalytic performance for soot oxidation was evaluated by temperature-programmed oxidation (TPO) of soot–catalyst mixtures so as to compare the CeO_2–Ag catalyst with other reference catalysts. Two kinds of carbon black powder (Degussa AG, Printex-V with BET surface area 85 m^2/g, and Degussa AG, Printex-U with BET surface area 92 m^2/g) were used as the model soot in this

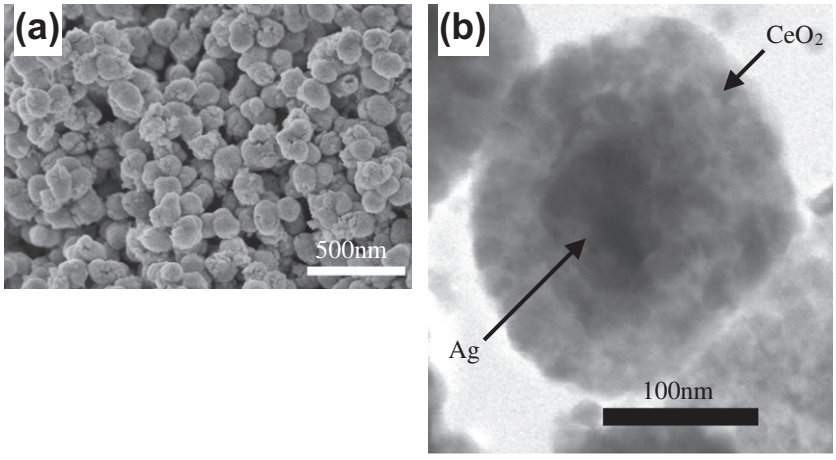

Fig. 1. (a) SEM image of CeO_2–Ag catalyst particles and (b) TEM image of the cut plane of a single spherical agglomerate of CeO_2–Ag catalyst [28].

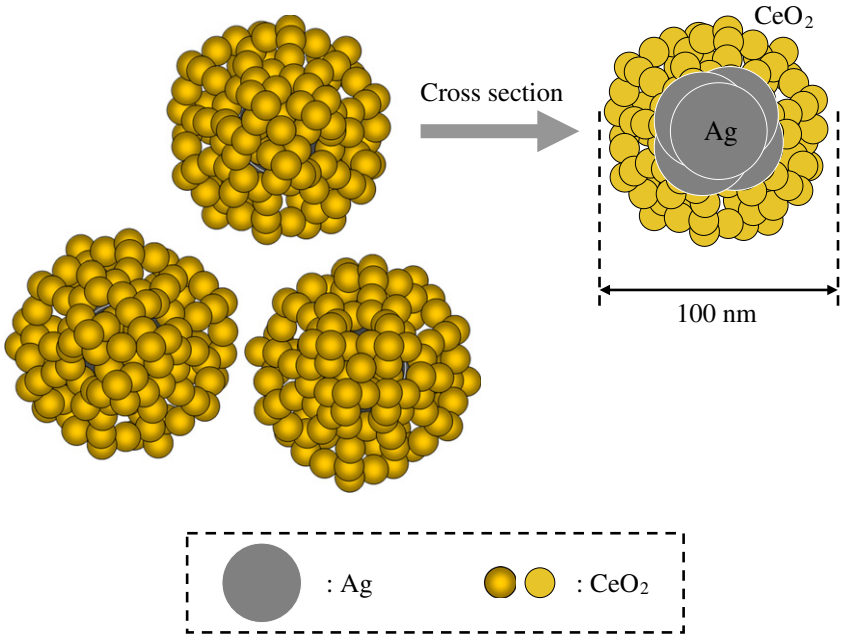

Fig. 2. Structural schematic of the CeO_2–Ag catalyst [28].

study. The tight contact and loose contact modes were adopted for the soot–catalyst mixture [1,6]. The tight contact was attained by grinding catalyst with Printex-V using a magnetically driven mortar for 5 min. The loose contact was achieved by mixing catalyst with Printex-U loosely using a spatula for 10 min in a reproducible way. Because the grain size of the Printex-U is smaller than that of the Printex-V, for a better contact between the soot and catalyst, the Printex-U was used for the samples in the loose contact mode. The weight ratios of the soot to catalyst were both 1:19.

In TPO experiments, the heat and mass transfer were concerned. Against heat and mass transfer limitations, two measures were taken as follows: for heat release from soot combustion, quartz wool (Tosoh, Fine grade) was used to dilute samples of catalyst–soot mixtures. For mass transfer limitation, the gas of 10% O_2/He was flowed at a relative high flow rate (50 mL/min), although just 40 mg of the soot–catalyst mixture was put in a fixed-bed flow reactor. The two measures ensured that there was no apparent temperature rises caused by soot oxidation, and mass transfer limitation could be ignored. So, we can say that the reaction regime was mostly controlled by the chemical kinetics, instead of by mass and heat transfer. A thermocouple was inserted into the soot–catalyst mixtures in order to monitor the reaction temperature. TPO spectra were recorded at a heating rate of 20 °C/min. The concentration of CO_2 and CO in the effluent was analyzed online using a quadrupole mass spectrometer (Q-MS; Ulvac, RG-102). Soot oxidation was regarded as the sum of the amount of CO_2 and CO formed during TPO; however, the amount of CO formed was much less than that of CO_2 in the presence of all of the catalysts examined. CO was only observed in the absence of the catalyst. The catalytic performance in this study is indicated by the temperature corresponding to the maximum soot oxidation rate (T_{max}) derived from the TPO spectra, with reference to the method by Moulijn et al. [1,6]. A lower T_{max} value indicates higher catalytic performance for soot oxidation.

2.3. Catalyst characterization

The BET surface area was measured by single-point N_2 adsorption at −196 °C using an automatic surface area analyzer (Microdata, MS4232II) after pretreatment at 200 °C for 20 min.

X-ray diffraction (XRD; Rigaku, RINT-TTR) patterns of the powder samples were recorded using Cu Kα radiation and a fixed power source (50 kV and 300 mA). The data were obtained between 20° and 60° (2θ) with a step of 0.02° and for 1 s per step. The average particle sizes of all the phases present in the catalysts were estimated using Scherrer's equation.

Oxygen temperature-programmed desorption (O_2-TPD) was performed in a fixed-bed reactor. For O_2 pre-adsorption, 160 mg of the catalyst was heated in a 20 mL/min O_2 flow at 600 °C for 30 min and cooled down to room temperature. After purging the catalyst with Ar for 30 min at room temperature, the catalyst was heated to 600 °C at 20 °C/min under a 20 mL/min Ar flow. The corresponding O_2 desorption spectrum was detected using the Q-MS.

Isotopic exchange (IE) reaction experiments were carried out in a re-circulated reactor (ca. 100 cm^3) coupled to the Q-MS. Masses of 32, 34, 36 (oxygen isotopomers, $^{16}O_2$, $^{18}O^{16}O$, and $^{18}O_2$), and 28 (to detect a possible leak) were continuously monitored. The vacuum connection to the mass spectrometer was thermoregulated to maintain a constant pressure of 10^{-4} Pa, while the pressure in the reactor loop was 5650 Pa. Thirty milligrams of the catalyst was placed into a quartz reactor for *in situ* experimentation. After oxidation with oxygen at 500 °C for 30 min and evacuation at 500 °C for 10 min, the sample was cooled to 300 °C; 5650 Pa of pure $^{18}O_2$ (99.2% of ^{18}O, ICON) was then introduced at 300 °C, and the partial pressure variation of the oxygen isotopomers, P_{36} ($^{18}O_2$), P_{34} ($^{18}O^{16}O$), and P_{32} ($^{16}O_2$), was continuously recorded. The total pressure (P_{36}, P_{34}, and P_{32}) remained virtually constant. A more detailed description of this experiment is given elsewhere [29,30]. From the partial pressure values, the ^{18}O atomic fraction $\alpha_g(t)$ in the gas phase at a time t can be defined as:

$$\alpha_g(t) = [(1/2)P_{34}(t) + P_{36}(t)]/[P_{36}(t) + P_{34}(t) + P_{32}(t)] \quad (1)$$

The IE reaction at a time t, IE(t), corresponds to the disappearance of ^{18}O from the gas phase; therefore, it is possible to determine IE(t) (in moles of oxygen molecules per catalyst weight) using the following equation [29]:

$$\begin{aligned} IE(t) &= n_g[1 - \alpha_g(t)]/w_c \\ &= (P_T/R)(V_r/T_r + V_c/T_c)[1 - \alpha_g(t)]/w_c \end{aligned} \quad (2)$$

where n_g is the total number of moles of oxygen molecules in the gas phase, w_c is the catalyst weight, P_T is the total pressure, R is the ideal gas constant, V_r and V_c are the volumes of the heated and unheated zones of the reactor, respectively, and T_r and T_c are the temperatures of the heated and unheated zones of the reactor, respectively. The rate of IE reaction (in moles of oxygen molecules per catalyst weight and per time unit), R_{IE}, can be calculated using the following equation:

$$R_{IE} = -(n_g/w_c)d\alpha_g(t)/dt = -(P_T/Rw_c)(V_r/T_r + V_c/T_c)d\alpha_g(t)/dt \quad (3)$$

ESR analysis was conducted using a Bruker ESP350E spectrometer at 9.46 GHz. Twenty milligrams of catalyst was placed in a 3.5-mm-diameter quartz ESR tube attached to a high-vacuum stopcock, which allowed pretreatment and adsorption of various gases. After pre-adsorption of O_2 at 600 °C for 30 min, the catalyst was cooled to room temperature, purged with He for 30 min, and then finally exposed to a He flow or 3% H_2/He flow at 50 mL/min for 2 min at 250 °C, while the ESR spectrum was recorded at 20 K. Technically, it is difficult to monitor or track the oxygen source involved in the soot oxidation. Considering the light-off temperature of soot oxidation (TPO) and oxygen desorption temperature from the O_2-TPD experiment, the above temperature of the ESR analysis was chosen as 250 °C. At this temperature, the existing oxygen species could be probed properly. Spin density was determined from double integration of derivative ESR signals and comparison with the weak pitch sample.

3. Results

3.1. Morphology and structural properties of catalysts

Fig. 3 shows XRD patterns of the CeO_2–Ag, Ag(39)/CeO_2, Ag(39)+CeO_2, Ag(39)/Al_2O_3, and CeO_2 catalysts, in addition to that of Ag powder used for the preparation of the Ag(x)+CeO_2 catalysts. The CeO_2–Ag catalyst consists of Ag (JCPDS 4-783) and CeO_2 (JCPDS 34-394) phases. The Ag(39)/CeO_2 and Ag(39)+CeO_2 catalysts also consist of Ag and CeO_2 phases. No evidence for the presence of the Ag_2O phase was obtained from the XRD patterns of all Ag-containing catalysts.

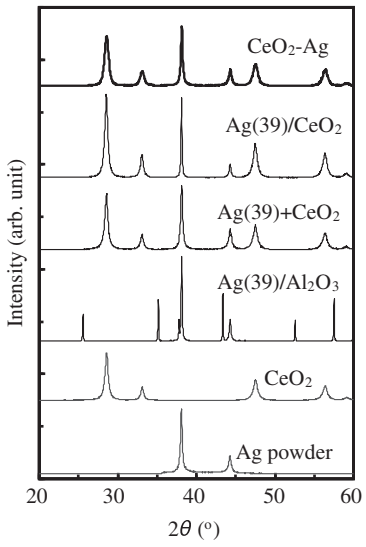

Fig. 3. XRD patterns of CeO_2–Ag, Ag(39)/CeO_2, Ag(39) + CeO_2, Ag(39)/Al_2O_3, and CeO_2 catalysts and Ag powder.

The particle sizes of the Ag and CeO_2 phases and lattice spacings of Ag(1 1 1) and CeO_2(1 1 1) calculated from the XRD patterns of the catalysts are summarized in Table 1. The lattice spacing of Ag(1 1 1) and CeO_2(1 1 1) in the CeO_2–Ag catalyst is consistent with that of Ag(1 1 1) in the Ag powder and that of CeO_2(1 1 1) in the CeO_2 catalyst, respectively. Thus, no solid reaction occurred between the Ag and CeO_2 phases in this catalyst. In a similar fashion, no solid reaction occurred in the Ag(x)/CeO_2 and Ag(x)+CeO_2 catalysts, irrespective of the Ag content. The particle sizes of the Ag (36 nm) and CeO_2 (16 nm) phases from the XRD patterns of the CeO_2–Ag catalyst are consistent with the TEM image (Fig. 1b).

3.2. TPO of catalyst–soot mixtures

Figs. 4a and 5a show the TPO profiles for soot oxidation over CeO_2–Ag, Ag(39)/CeO_2, Ag(39)+CeO_2, Ag(39)/Al_2O_3, and CeO_2 catalysts carried out under 10% O_2/He flow in addition to that for non-catalyzed soot oxidation (without catalyst) in tight and loose contact modes, respectively. The TPO profiles for all catalysts were shifted to lower temperatures compared with non-catalyzed soot oxidation regardless of the contact mode, which confirms that all the catalysts are able to catalyze soot oxidation. The performances of the CeO_2–Ag, Ag(39)/CeO_2, and Ag(39)+CeO_2 catalysts are higher than those of the Ag(39)/Al_2O_3 and CeO_2 catalysts in both contact modes. This result indicates that the catalytic performance for soot oxidation is promoted by the combination of Ag and CeO_2 particles. Moreover, the CeO_2–Ag catalyst exhibits much higher catalytic performance than the Ag(39)/CeO_2 and Ag(39)+CeO_2 catalysts, conventionally supported and mixed with the same composition respectively, in both contact modes.

Figs. 4b and 5b show TPO profiles for soot oxidation over Ag(x)/CeO_2 catalysts with different Ag contents in tight and loose contact modes, respectively. Figs. 4c and 5c show TPO profiles for soot oxidation over Ag(x)+CeO_2 catalysts with different Ag contents in tight and loose contact modes, respectively. The derived T_{max} values of the all catalysts in both contact modes are summarized in Table 2. For all the catalysts, the order of soot oxidation performance in tight contact mode is almost the same to that in loose contact mode. The Ag(10)/CeO_2 catalyst has the highest performance among the Ag(x)/CeO_2 catalysts, and the Ag(10)+CeO_2 catalysts have the highest performance among the Ag(x)+CeO_2 catalysts, in both contact modes. However, the Ag(10)/CeO_2 and Ag(10)+CeO_2 catalysts are both inferior in performance to the CeO_2–Ag catalyst. On the other hand, the advantage with the Ag(10)+CeO_2 catalysts is its very simple preparation procedure.

The Ag(1.9)/CeO_2 catalyst has lower performance than the Ag(1.9)+CeO_2 catalyst with the same composition in both contact modes (Table 2), while the former catalyst has smaller Ag particles (Table 1) and therefore a larger Ag surface area than the latter catalyst. The Ag(0.95)/CeO_2 and Ag(0.95)+CeO_2 catalysts exhibit the same trend in catalytic performance and Ag particle size, which suggests that smaller Ag particles do not necessarily cause higher catalytic performance for soot oxidation.

All the catalysts show lower performance for soot oxidation in loose contact mode than that in tight contact mode. The contact closeness between catalyst and soot is very important for the soot oxidation activity over a catalyst [6]. Even in the loose contact mode, the CeO_2–Ag catalyst still exhibits the highest performance among the catalysts, soot oxidation starting around 280 °C and revealing its T_{max} at 376 °C. Moreover, the CeO_2–Ag shows the smallest T_{max} difference between loose and tight contact modes (ΔT_{max} values in Table 2) among the all catalysts, that is, the CeO_2–Ag catalyst is the most insensitive to the physical contact mode between soot and catalyst.

The TPO experiment was repeated with the used CeO_2–Ag catalyst. As illustrated in Figs. 4a and 5a corresponding to tight and

Table 1
Morphology and structural properties of catalysts; BET surface area, particle size, and lattice spacing.

Catalyst	BET surface area (m^2/g)	Particle size (nm)		Lattice spacing (nm)		Peak intensity ratio (–) Ag(1 1 1)/CeO_2(1 1 1)
		Ag	CeO_2	Ag(1 1 1)	CeO_2(1 1 1)	
CeO_2–Ag	14.7	36	16	0.2358	0.3121	0.73
Ag(39)/CeO_2	30.1	89	21	0.2359	0.3124	0.37
Ag(10)/CeO_2	52.0	60	20	0.2359	0.3121	0.11
Ag(3.2)/CeO_2	59.2	28	20	0.2359	0.3122	0.03
Ag(1.9)/CeO_2	70.0	20	20	0.2356	0.3121	0.02
Ag(0.95)/CeO_2	78.1	n.d.[a]	20	–	0.3120	–
Ag(39)+CeO_2	49.9	47	20	0.2358	0.3120	0.85
Ag(10)+CeO_2	72.0	35	20	0.2358	0.3122	0.14
Ag(3.2)+CeO_2	77.2	31	20	0.2358	0.3122	0.05
Ag(1.9)+CeO_2	77.7	32	20	0.2359	0.3122	0.04
Ag(0.95)+CeO_2	78.0	34	20	0.2355	0.3120	0.02
Ag(39)/Al_2O_3	12.7	48	–	0.2359	–	–
CeO_2	77.8	–	20	–	0.3120	–
Ag powder	9.6	34	–	0.2359	–	–

[a] n.d.: not detected.

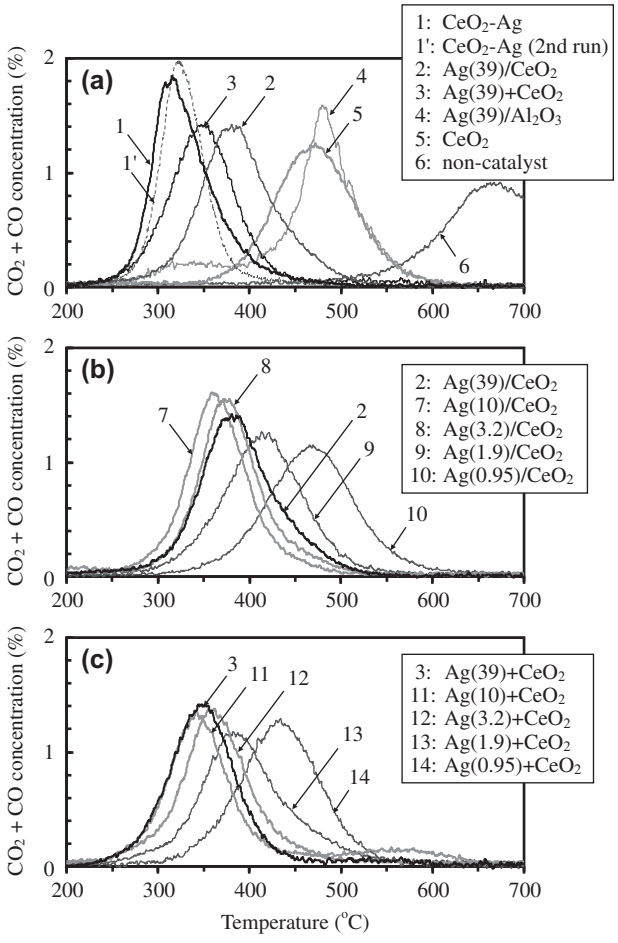

Fig. 4. (a) TPO profiles for soot oxidation in the presence and absence of CeO_2–Ag, Ag(39)/CeO_2, Ag(39) + CeO_2, Ag(39)/Al_2O_3, CeO_2 catalysts in tight contact mode. (b and c) TPO profiles for soot oxidation in the presence of Ag(x)/CeO_2 and Ag(x) + CeO_2 catalysts in tight contact mode.

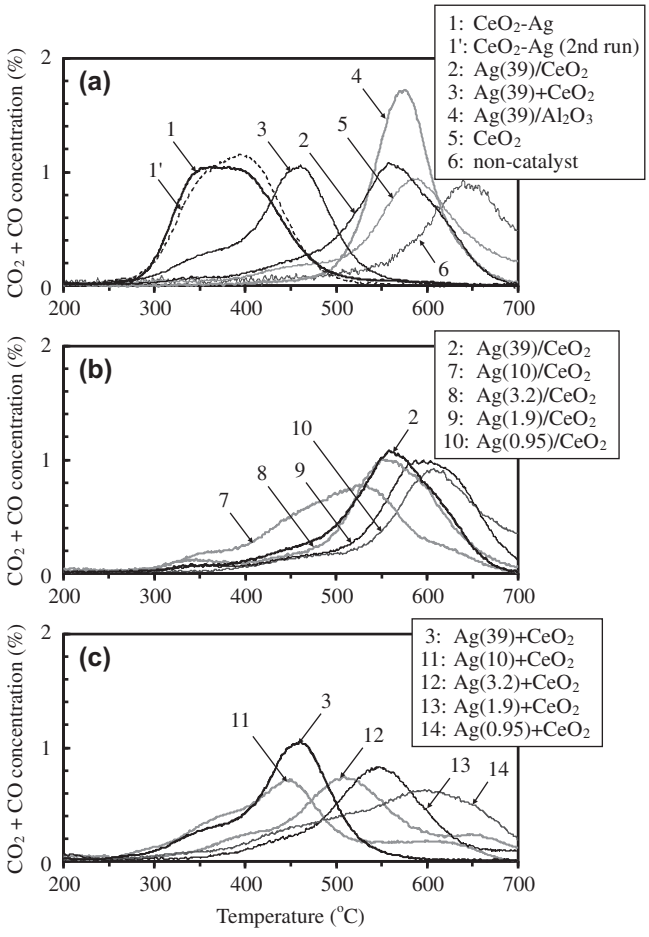

Fig. 5. (a) TPO profiles for soot oxidation in the presence and absence of CeO_2–Ag, Ag(39)/CeO_2, Ag(39) + CeO_2, Ag(39)/Al_2O_3, CeO_2 catalysts in loose contact mode. (b and c) TPO profiles for soot oxidation in the presence of Ag(x)/CeO_2 and Ag(x) + CeO_2 catalysts in loose contact mode.

loose contact modes, the TPO profile with the repeated experiment (curve 1′) exhibits almost the same catalytic performance to that with the first TPO run in both contact modes. This result indicates that the soot oxidation activity of the CeO_2–Ag catalyst is almost reproducible, and the CeO_2–Ag catalyst has the potential for future actual application. It was also noted that the second spectrum slightly shifted to higher temperatures in all cases. This indicated that the CeO_2–Ag catalyst somewhat deteriorated after experienced the first test. It is assumed that the rice-ball morphology of the CeO_2–Ag subtly collapses during the soot oxidation, or some unburned fine soot particles and ash generated in the first run caused bad contact between the used catalyst and fresh soot.

Table 2
Catalytic performance for soot oxidation and parameters from O_2-TPD, $^{18}O/^{16}O$ IE reaction, and ESR experiments.

Catalyst	T_{max} (°C)		ΔT_{max}[a] (°C)	O_2 desorption (μmol/g)	IE reaction rate (μmol/g min)	Spin density (μmol/g)
	Tight contact	Loose contact				
CeO_2–Ag	315	376	61	33.5	22.6	0.830
Ag(39)/CeO_2	381	563	182	9.1	9.1	0.232
Ag(10)/CeO_2	362	526	164	17.0	12.9	0.465
Ag(3.2)/CeO_2	371	550	179	9.3	7.4	–
Ag(1.9)/CeO_2	414	596	182	2.1	3.9	–
Ag(0.95)/CeO_2	466	610	144	0.5	–	–
Ag(39) + CeO_2	351	461	110	23.5	–	–
Ag(10) + CeO_2	342	443	101	25.0	–	–
Ag(3.2) + CeO_2	355	522	167	18.0	–	–
Ag(1.9) + CeO_2	384	548	164	5.0	6.4	–
Ag(0.95) + CeO_2	433	597	164	1.9	–	–
Ag(39)/Al_2O_3	480	575	95	2.0	2.7	0.091
CeO_2	462	590	128	0.0	0.6	0.002
None (soot only)	660[b]	640[c]	–		–	–

[a] ΔT_{max} = (T_{max} in loose contact mode) – (T_{max} in tight contact mode).
[b] T_{max} of Printex-V.
[c] T_{max} of Printex-U.

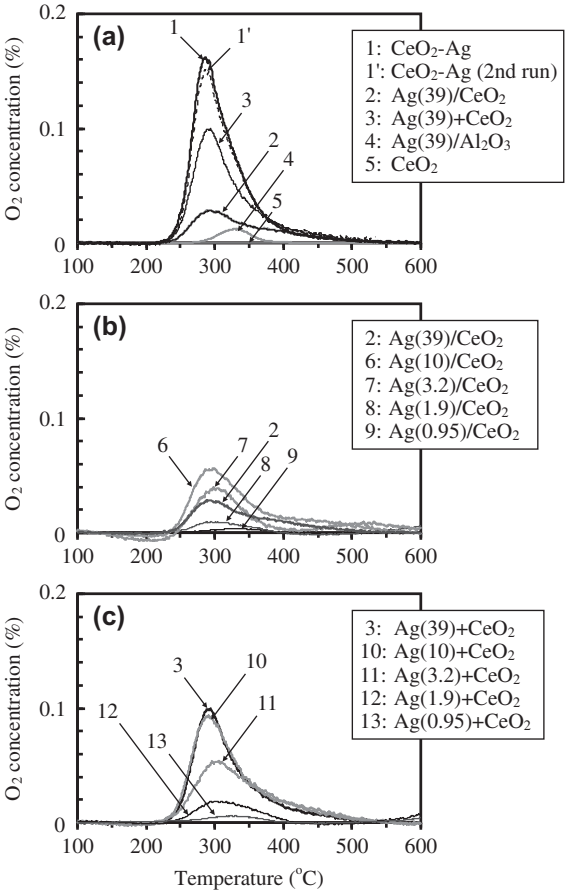

Fig. 6. (a) O_2-TPD profiles of CeO_2–Ag, Ag(39)/CeO_2, Ag(39) + CeO_2, Ag(39)/Al_2O_3, CeO_2 catalysts. (b and c) O_2-TPD profiles of Ag(x)/CeO_2 and Ag(x) + CeO_2 catalysts.

Further investigations are necessary to clarify the involved reasons for this deactivation, as well as more efforts to improve its thermostability.

3.3. O_2-TPD

Fig. 6a–c show O_2-TPD profiles of the CeO_2–Ag and reference catalysts. The CeO_2–Ag catalyst exhibits O_2 desorption between 200 and 450 °C, corresponding to the light-off of soot oxidation below 300 °C over the CeO_2–Ag catalyst (Figs. 4a and 5a). O_2 desorption is also observed from the Ag(x)/CeO_2, Ag(x)+CeO_2, and Ag(39)/Al_2O_3 catalysts in the same temperature range, but not for the CeO_2 catalyst.

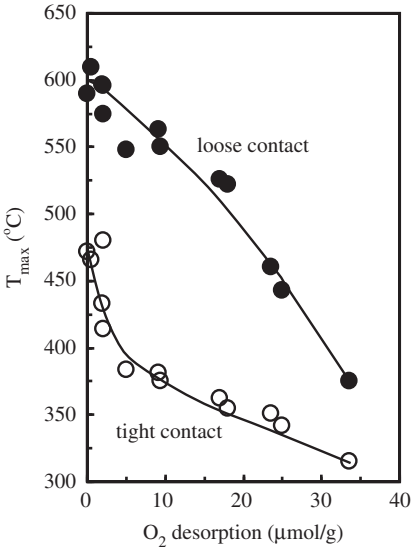

Fig. 7. T_{max} value from TPO experiments in tight and loose contact modes as a function of the amount of O_2 desorption determined from O_2-TPD experiments.

The amounts of O_2 desorption from the catalysts between 200 and 450 °C are summarized in Table 2. The CeO_2–Ag catalyst exhibits the largest O_2 desorption among all the catalysts. Fig. 7 reveals an excellent correlation between the T_{max} values for TPO in tight and loose contact modes, respectively, as a function of the amounts of O_2 desorption from O_2-TPD over all the catalysts. These results strongly suggest that active oxygen species for soot oxidation correspond to the adsorbed oxygen species on the catalyst from gaseous O_2, which is desorbed in the temperature range between 200 and 450 °C.

The O_2-TPD experiment was also repeated with the used CeO_2–Ag catalyst. As indicated in Fig. 6a, almost the same O_2-TPD spectra of the CeO_2–Ag catalyst were gained in first and second runs. This result demonstrates that the gaseous oxygen could be adsorbed

onto the CeO_2–Ag catalyst and activated to active oxygen species in a reproducible way.

3.4. $^{18}O/^{16}O$ IE reaction

The IE reaction as a informative technique was employed to characterize oxygen mobility over the catalysts [29,30] in this study. As shown in Fig. 8a, the partial pressures of three oxygen molecules, P_{36} ($^{18}O_2$), P_{34} ($^{18}O^{16}O$), and P_{32} ($^{16}O_2$), evolve during the $^{18}O/^{16}O$ IE reaction over the CeO_2–Ag catalyst at 300 °C. The $^{18}O_2$ molecules in the gas phase adsorb and decompose on the catalyst surface and then exchange and desorb to $^{18}O^{16}O$ and $^{16}O_2$ molecules into the gas phase. Fig. 8b and c show IE reaction profiles against reaction time over the CeO_2–Ag and reference catalysts derived by Eq. (2). At 300 °C, the IE reaction proceeds the fastest over the CeO_2–Ag catalyst, apparently occurs over the Ag(x)/CeO_2, Ag(x)+CeO_2, and Ag(39)/Al_2O_3 catalysts, but is detectable over the CeO_2 catalyst, indicating that the co-existence or inter-particle contact of Ag particle and CeO_2 is truly necessary for the IE reaction or oxygen migration.

The initial IE reaction rates by Eq. (3) are summarized in Table 2. The CeO_2–Ag catalyst shows higher IE reaction rate than the Ag(x)/CeO_2, Ag(x)+CeO_2, Ag(39)/Al_2O_3, and CeO_2 catalysts. The IE reaction rates or migration rate closely associates with oxygen species adsorbing and migrating on Ag surface, the interface between Ag and CeO_2, and the surface and bulk of CeO_2. These results above reveal that the active oxygen species are potentially mobile from the gaseous O_2 onto the Ag surface through adsorption and actively

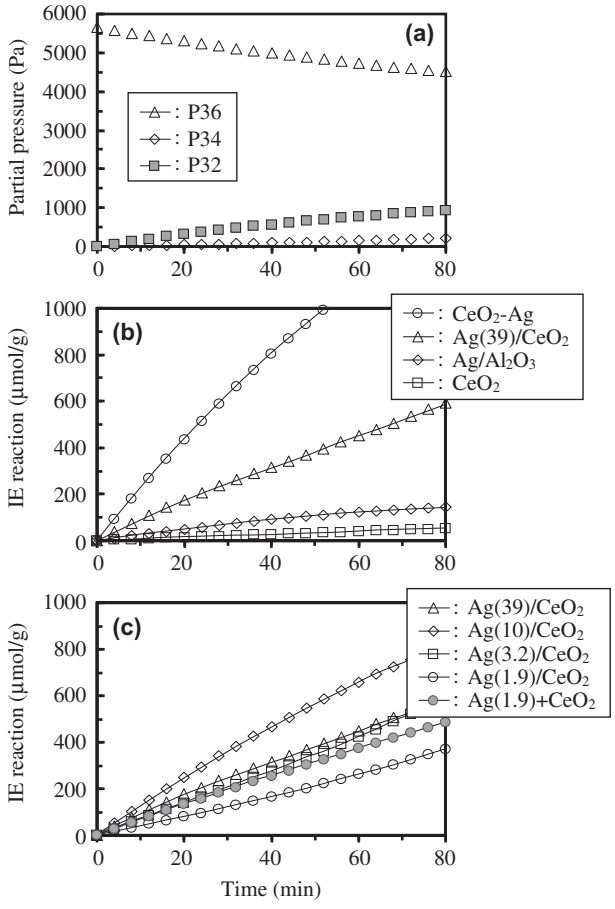

Fig. 8. (a) Partial pressure evolution of $^{18}O_2$, $^{18}O^{16}O$, and $^{16}O_2$ molecules for the IE reaction over the CeO_2–Ag catalyst at 300 °C. (b) IE reaction profiles of CeO_2–Ag, Ag(39)/CeO_2, Ag(39)/Al_2O_3, CeO_2 catalysts. (c) IE reaction profiles of Ag(x)/CeO_2 and Ag(x) + CeO_2 catalysts.

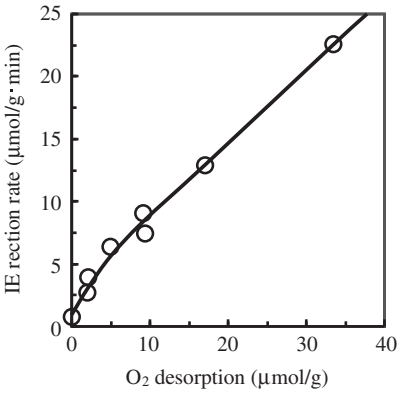

Fig. 9. IE reaction rates for the $^{18}O/^{16}O$ IE reaction versus the amount of O_2 desorption determined from O_2-TPD experiments.

exchangeable with the oxygen in CeO_2, bridged by the interface between the Ag and the CeO_2 particles of the catalysts. As the result, the CeO_2–Ag catalyst with the unique "rice-ball" morphology exhibits the fastest oxygen migration via the interface between the Ag and the CeO_2 particles among all the catalyst samples.

Fig. 9 shows a good correlation between the IE reaction rates for the $^{18}O/^{16}O$ IE reaction and the amounts of O_2 desorption from O_2-TPD measurements.

3.5. ESR

When CeO_2–Ag catalyst is exposed to He flow at 200 °C after a pretreatment (exposure to O_2 flow at 600 °C for 30 min, cooling to room temperature under the same gas flow and exposure to He flow for 30 min at room temperature), no ESR signals of oxygen species were observed. However, when exposed to 3% H_2/N_2 flow at 200 °C for 2 min after the same pretreatment, ESR signals with $g_{//} = 2.046$, $g_{//} = 2.037$, and $g_{\perp} = 2.010$ were observed, as shown in Fig. 10. These signals are all attributed to superoxide (O_2^-) species bonded to Ce cations [31,32]. ESR analyses of other catalysts using the same procedure also provide signals with the same g values. Among all of the catalysts shown in Fig. 9, the CeO_2–Ag catalyst shows the highest ESR signal intensity.

The spin densities of O_2^- species over the catalysts are listed in Table 2. Fig. 11 shows a linear correlation between the spin

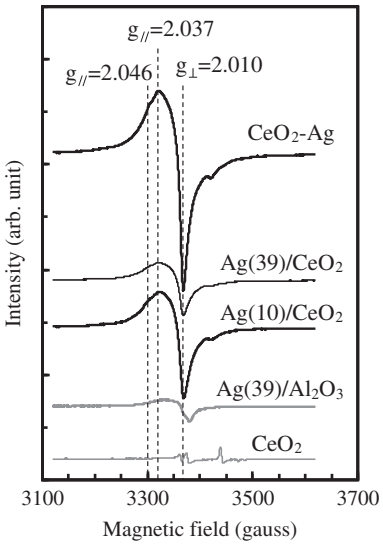

Fig. 10. ESR spectra of CeO_2–Ag, Ag(39)/CeO_2, Ag(10)/CeO_2, Ag(39)/Al_2O_3, CeO_2 catalysts.

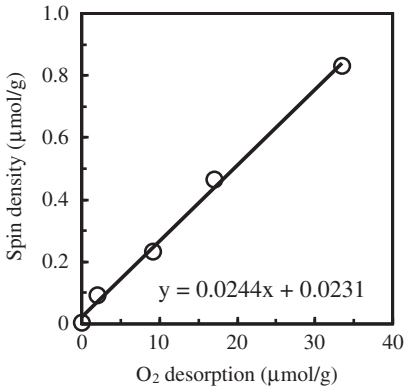

Fig. 11. Spin densities of O_2-species versus the amount of O_2 desorption from O_2-TPD experiments.

densities of O_2^- species from ESR and the amount of O_2 desorption from O_2-TPD with a slope of 0.024, which indicates that some part of the adsorbed oxygen species on the catalyst under oxidative conditions are transformed into the O_2^- species on the CeO_2 surface under weak reductive conditions.

4. Discussion

4.1. Effect of rice-ball morphology on the formation of active oxygen species for soot oxidation

The CeO_2–Ag catalyst with a rice-ball morphology exhibits higher performance for soot oxidation than any of the conventional supported Ag(x)/CeO_2, Ag(x)+CeO_2 mixed, Ag(x)/Al_2O_3, and CeO_2 catalysts, irrespective of the Ag content and the tight or loose mode of the soot–catalyst contact. An excellent correlation between soot oxidation performance and the amount of O_2 desorption from O_2-TPD (Fig. 7) strongly suggests that active oxygen species for soot oxidation correspond to the oxygen species adsorbed on the catalyst from gaseous O_2 and desorbed from 200 to 450 °C. That is, the amount of O_2 desorption from O_2-TPD is parallel to the amount of the active oxygen species formed on the catalyst. Therefore, the increased performance of the CeO_2–Ag catalyst is closely relevant to the promoted formation of the active oxygen species compared to the other catalysts. In this section, we explore the reasons for the ease and extent of active oxygen species formation over the CeO_2–Ag catalyst.

It was reported that atomic oxygen species on Ag surfaces desorb as molecular O_2 around 300 °C [33–36]. There is no O_2 desorption in the O_2-TPD spectrum of CeO_2 catalyst, Therefore, the atomic oxygen species are very likely formed on the Ag surface by adsorption from gaseous O_2 and activated to participate into soot oxidation as active oxygen species. On the other hand, the Ag(39)/CeO_2 catalyst has a much larger amount of O_2 desorption from O_2-TPD than the Ag(39)/Al_2O_3 catalyst, while the former has larger Ag particles and consequently a smaller Ag surface than the latter (Tables 1 and 2). This suggests that a synergistic effect from the Ag–CeO_2 combination contributes to the formation of active oxygen species on the Ag surface. This synergistic effect is caused by the interface between Ag and CeO_2 particles, not merely the physical factor of Ag dispersion on the supporting material [31]. Thus, the interface between Ag and CeO_2 particles plays a crucial role in catalytic soot oxidation. A good correlation is obtained between the amount of active oxygen species formed on the Ag surface and the rate of oxygen migration via the interface between Ag and CeO_2 particles (Fig. 9). Lippits et al. reported that the interaction between Ag and CeO_2 has a significant influence on the activity for the selective oxidation of ammonia to nitrogen, possibly due to an improved supply of active oxygen from the CeO_2 to Ag particles [37]. Therefore, it is reasonable to conclude that the larger interface between Ag and CeO_2 particles leads to increased formation of active oxygen species on the Ag surface possibly due to a faster supply of oxygen from the CeO_2 to Ag particles and the stabilization of oxygen on the Ag surface [26].

Next, we consider the effect of Ag particle size on the formation of active oxygen species for soot oxidation. With respect to the interface between Ag and CeO_2 particles, small Ag particles loaded on the CeO_2 surface are expected to create a large interface area; however, the Ag(1.9)/CeO_2 catalyst with smaller Ag particles has lower O_2 desorption from O_2-TPD compared to the Ag(1.9)+CeO_2 catalyst with larger Ag particles (Table 1 and 2). The Ag(0.95)/CeO_2 catalyst, with a Ag particle size too small to be determined by XRD, and the Ag(0.95)+CeO_2 catalyst exhibit the same trend between the formation of active oxygen species and the Ag particle size, which indicates that small Ag particles of 20 nm or less are unfavorable for the formation of the active oxygen species on their surfaces.

Many authors have reported catalytic size effects over supported Ag catalysts for some reactions, such as ethylene epoxidation, propylene epoxidation, and methane oxidation [38–43]. Bal'zhinimaev, using Ag/Al_2O_3 and Ag/SiO_2 catalysts with the average Ag particle sizes between 15 and 2000 nm, showed that the specific rate of ethylene epoxidation drastically increased by more than one order of magnitude with an increase in the size of the Ag particles from 20 to 50 nm and a further slight increase with further increase in the size of the Ag particles [38]. Bal'zhinimaev demonstrated that nucleophilic oxygen species, formed via dissociative chemisorption of O_2 molecules, and electrophilic oxygen species, formed from nucleophilic oxygen species, play cooperative roles in the reaction. Nucleophilic oxygen species are formed on a regular surface region, which is obtained by large Ag particles. Both nucleophilic and electrophilic oxygen species are atomic oxygen species adsorbed on the Ag surface. Therefore, it is very likely that the formation of active oxygen species for soot oxidation is also favored by large Ag particles greater than a certain size. On the other hand, Ag particles that are too large are expected to impede the formation of active oxygen species, due to their small surface area and small interface area formed with CeO_2 particles. The Ag(10)/CeO_2 catalyst with larger Ag particles (60 nm) has less O_2 desorption than the Ag(10)+CeO_2 catalyst with smaller Ag particles (35 nm) (Tables 1 and 2). Therefore, it may be that active oxygen species for soot oxidation is formed most effectively on Ag particles with sizes in the range between 30 and 40 nm.

A large interface between moderately large Ag particles (probably > 30 nm) and CeO_2 particles can be achieved by the deposition of fine CeO_2 particles that are much smaller than Ag particles on the Ag surface, that is, a rice-ball morphology. The amount of active oxygen species formed on the Ag surface in the CeO_2–Ag catalyst is 67 μmol oxygen atoms/g derived from the O_2 desorption (Table 2). The number of exposed Ag atoms in the CeO_2–Ag catalyst as derived from the Ag particle size (36 nm) from XRD measurements is 52 μmol Ag atoms/g (Table 1). This number might be underestimated, because XRD measurement detects larger Ag particles preferentially in the case of a size distribution of Ag particles. Thus, we may say that the number of exposed Ag atoms is comparable to the amount of the active oxygen species formed on the Ag surface. Therefore, these results suggest that the active oxygen species for soot oxidation is effectively formed on most of the exposed Ag atoms and an extremely large interface of the Ag surface with CeO_2 particles results from the rice-ball morphology of the CeO_2–Ag catalyst.

It is concluded that the rice-ball morphology of the CeO_2–Ag catalyst is optimal for the formation of active oxygen species for soot oxidation, because it satisfies the requirement for both mod-

erately large Ag particles (ca. 30–40 nm) and an extremely large interface area with CeO_2 particles.

4.2. Effect of rice-ball morphology on the migration of active oxygen species for soot oxidation

The soot used in this study cannot physically contact the Ag particles in the center of the CeO_2–Ag catalyst particles, because the particle size (ca. 100 nm) is too large, and soot oxidation proceeds efficiently on the CeO_2 surface surrounding the spherical agglomerate. Therefore, it is supposed that the active oxygen species generated on the Ag surface from gaseous O_2 migrates to soot particles on the CeO_2 surface during soot oxidation. In this section, we investigate the migration of the active oxygen species for soot oxidation over the CeO_2–Ag catalyst.

ESR analyses show that some atomic oxygen species adsorbed on the Ag surface from gaseous O_2 under oxidative conditions are transformed into O_2^- species on the CeO_2 surface under weak reductive conditions (Fig. 11). It is known that the catalyst is exposed to local reductive conditions during soot oxidation [20]. Thus, it is likely that the active oxygen species formed on the Ag surface of the CeO_2–Ag catalyst migrate via the interface between Ag and CeO_2 particles to the CeO_2 surface, of which a certain fraction are transformed into the O_2^- species during soot oxidation. Surface mobility phenomena of active oxygen species on CeO_2-containing oxides have been invoked by many authors and considered as an elementary step of the reaction mechanisms [17,29,30,44–46]. Martin et al. reported that the reoxidation of pre-reduced CeO_2 proceeds with very mobile oxygen species and leads to an excess of oxygen uptake due, in particular, to the presence of different oxygen species, which could be superoxide (O_2^-) and peroxide (O_2^{2-}) species [46]. Krishna et al. reported that CeO_2 and rare-earth-modified CeO_2 catalysts function to increase active oxygen transfer to the soot surface, followed by chemisorption of the active oxygen to form surface oxygen complexes during soot oxidation [17]. Therefore, it is very likely that active O_n^{x-} species ($n = 1$ or 2, $x = 1$ or 2) on the CeO_2 surface of the CeO_2–Ag catalyst also migrate onto the soot particles for soot oxidation. Most of the O_n^{x-} species would be O_2^-, although there remains the possibility for the presence of other oxygen species.

In general, the interface area between Ag and CeO_2 is smaller than the Ag and CeO_2 surface areas in catalysts composed of Ag and CeO_2 particles, which result in a bottleneck for the migration of oxygen species. In this case, transformation of the active oxygen species is required at the interface. Therefore, migration via the interface should be a rate determining step for the complete migration of the active oxygen species during soot oxidation. $^{18}O/^{16}O$ IE reactions reveal that the CeO_2–Ag catalyst exhibits the fastest oxygen migration via the interface (Fig. 8b and c). The interface area between the Ag and CeO_2 particles in the present CeO_2–Ag catalyst is extremely large; therefore, it can be concluded that the rice-ball morphology is also suitable for the fast migration of active oxygen species for soot oxidation. Two functions of the interface, faster migration and increased formation of the active oxygen species, were confirmed by the good correlation in Fig. 9.

4.3. Mechanism of soot oxidation over CeO_2–Ag catalyst

We propose a possible mechanism for soot oxidation over the CeO_2–Ag catalyst, depicted in Fig. 12, that illustrates the morphology of the catalyst. First, gaseous O_2 is adsorbed on the surface of Ag particles through a synergistic effect with CeO_2 particles to form atomic oxygen species, which are the first active oxygen species for soot oxidation. The extremely large interface between Ag and CeO_2 particles and the moderately large size of the Ag particles contribute to the formation of the species. The atomic oxygen species on the Ag surface then migrate to the surface of CeO_2 particles via the interface, transforming into O_n^{x-} species (at least partly O_2^-), which is the second active oxygen species. The extremely large interface contributes to the fast migration of the species. The first and second active oxygen species exist in equilibrium during soot oxidation. Finally, the O_n^{x-} species on the CeO_2 surface, which is a mobile active oxygen species, migrates onto the soot particle surfaces through the contact surface between CeO_2 and soot particles, oxidizes the soot completely to CO_2, and finally releases into the gas phase. The mobile active oxygen species abundantly formed in the interior portion of catalyst, migrate fast out to the external surface, and efficiently access to soot particles. This results in its outstanding catalytic performance for soot oxidation, but insensitivity to the contact between catalyst and soot.

Good correlations between the catalytic performance for soot oxidation and all parameters concerning the active oxygen species of catalysts in this study (Figs. 7, 9 and 11) demonstrate that the mechanism for soot oxidation over Ag(x)/CeO_2, conventional supported catalysts, and Ag(x)+CeO_2, particle mixed catalysts should be the same as that over the CeO_2–Ag catalyst, assuming that the

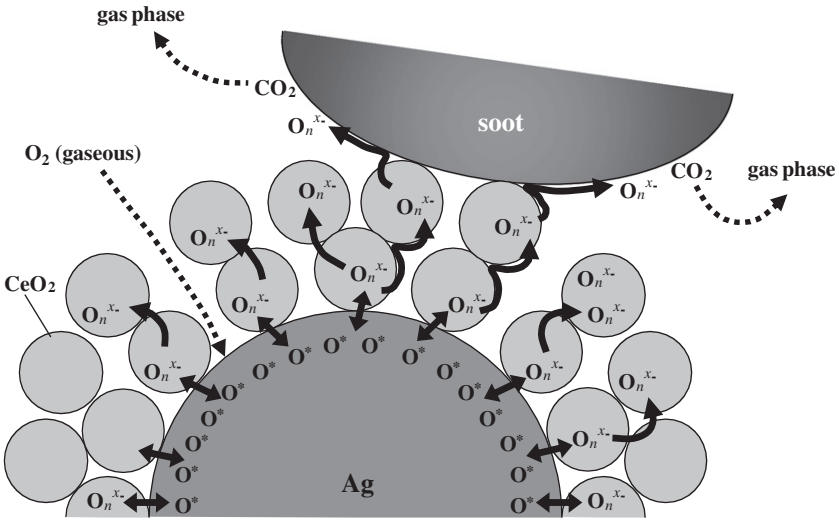

Fig. 12. Schematic mechanism for soot oxidation over the CeO_2–Ag catalyst.

Ag and CeO_2 particles and their interface have the same functions. Some researchers have suggested mechanisms for soot oxidation over Ag(x)/CeO_2 catalysts; however, they require further information, such as the mobility of the active oxygen species, the respective role of Ag and CeO_2 particles, and the factors influencing the activity for soot oxidation. By employing the rice-ball morphology in a CeO_2–Ag catalyst, the configuration of Ag, CeO_2, and soot particles can be set, which assists in understanding the mechanism of soot oxidation over the Ag(x)/CeO_2 and CeO_2–Ag catalysts.

On the other hand, the CeO_2 catalyst does not desorb O_2, as determined from O_2-TPD experiments; however, it does have some catalytic performance for soot oxidation (Figs. 4a and 5a). Several researchers have studied CeO_2 and rare-earth-modified CeO_2 catalysts for soot oxidation and have proposed mechanisms for soot oxidation over these catalysts that are based on their oxygen storage and release capacities [16–21] and should therefore be different from that over the CeO_2–Ag catalyst, although such mechanisms may be involved in the case of the CeO_2–Ag catalyst.

5. Conclusion

An innovative CeO_2–Ag catalyst with a unique agglomeration morphology similar to a rice-ball, which consists of a central Ag particle agglomerate surrounded by fine CeO_2 particles, exhibits outstanding performance for soot oxidation with gaseous O_2 below 300 °C in tight and loose contact modes. The catalytic performance is higher than those of conventional Ag/CeO_2 supported catalysts and of Ag+CeO_2 mixed particle catalysts irrespective of the Ag content, in addition to those of Ag/Al_2O_3 and CeO_2 catalysts, in both contact modes. Moreover, the CeO_2–Ag catalyst is less sensitive to contact between catalyst and soot than the other reference catalysts.

The reaction mechanism and high performance for soot oxidation over the CeO_2–Ag catalyst were investigated. O_2-TPD experiments show that atomic oxygen species adsorbed weakly on the Ag surface through a synergistic effect with CeO_2 particles from gaseous O_2, which are desorbed in the temperature range between 200 and 450 °C, function as active oxygen species for soot oxidation. $^{18}O/^{16}O$ IE reaction experiments revealed that atomic oxygen species on the Ag surface can migrate to the CeO_2 particles via the Ag/CeO_2 interface. ESR analysis indicated that some of the atomic oxygen species on the Ag surface migrate to the CeO_2 surface and transform into O_n^{x-} species ($n = 1$ or 2, $x = 1$ or 2, at least partly O_2^- species) during soot oxidation. These results suggest that the O_2^- species on the CeO_2 surface also function as the active oxygen species for soot oxidation. A possible mechanism for soot oxidation was proposed, where the active oxygen species formed on the Ag surface from gaseous O_2 migrate to the CeO_2 surface via the interface, transform into O_n^{x-} species, and then further migrate onto soot particles where oxidation occurs. The abundantly formed O_n^{x-} species migrate fast out to the external surface and efficiently access to soot particles. This is the key factor for its distinguished soot oxidation performance and insensitivity to the contact between catalyst and soot.

The CeO_2–Ag catalyst shows the abundant formation of active oxygen species due to the compatibility of the moderately large Ag particles (ca. 30–40 nm) and the extremely large interface area between the Ag and the CeO_2 particles due to the rice-ball morphology. This catalyst also exhibits fast migration of the active oxygen species due to the extremely large interface area. Therefore, it is concluded that the rice-ball morphology of the CeO_2–Ag catalyst is optimal for the formation and migration of active oxygen species for soot oxidation.

Acknowledgments

The authors thank K. Domen at the Department of Chemical System Engineering, The University of Tokyo, for helpful discussions.

References

[1] B.A.A.L. van Setten, M. Makkee, J.A. Moulijn, Catal. Rev. Sci. Eng. 43 (2001) 489.
[2] K. Hinot, H. Burtscher, A.P. Weber, G. Kasper, Appl. Catal. B 71 (2007) 271.
[3] B.J. Cooper, J.E. Thoss, SAE Paper 890404, 1989.
[4] K.N. Pattas, C.C. Michalopoulou, SAE Paper 920362, 1992.
[5] G. Lepperhoff, H. Luders, P. Barthe, J. Lemaire, SAE Paper 950369, 1995.
[6] J.P.A. Neeft, M. Makkee, J.A. Moulijn, Appl. Catal. B 8 (1996) 57.
[7] C. Badini, G. Saracco, V. Serra, Appl. Catal. B 11 (1997) 307.
[8] G. Saracco, C. Badini, N. Russo, V. Specchia, Appl. Catal. B 21 (1999) 233.
[9] G. Neri, G. Rizzo, S. Galvagno, A. Donato, M.G. Musolino, R. Pietropaolo, Appl. Catal. B 42 (2003) 381.
[10] H. An, C. Kilroy, P.J. McGinn, Catal. Today 98 (2004) 423.
[11] C.A. Querini, L.M. Cornaglia, M.A. Ulla, E.E. Miro, Appl. Catal. B 20 (1999) 165.
[12] M.L. Pisarello, V. Milt, M.A. Peralta, C.A. Querini, E.E. Miro, Catal. Today 75 (2002) 465.
[13] R. Jimenez, X. Garcia, C. Cellier, P. Ruiz, A.L. Gordon, Appl. Catal. A 314 (2006) 81.
[14] D. Fino, N. Russo, G. Saracco, V. Specchia, J. Catal. 217 (2003) 367.
[15] B.A.A.L. van Setten, C.G.M. Spitters, J. Bremmer, A.M.M. Mulders, M. Makkee, J.A. Moulijn, Appl. Catal. B 42 (2003) 337.
[16] A. Bueno-Lopez, K. Krishna, M. Makkee, J.A. Moulijn, J. Catal. 230 (2005) 237.
[17] K. Krishna, A. Bueno-Lopez, M. Makkee, J.A. Moulijn, Appl. Catal. B 75 (2007) 189.
[18] K. Krishna, A. Bueno-Lopez, M. Makkee, J.A. Moulijn, Appl. Catal. B 75 (2007) 210.
[19] E. Aneggi, M. Boaro, C. de Leitenburg, G. Dolcetti, A. Trovarelli, Catal. Today 112 (2006) 94.
[20] E. Aneggi, M. Boaro, C. de Leitenburg, G. Dolcetti, A. Trovarelli, J. Alloys Compd. 408-412 (2006) 1096.
[21] E. Aneggi, C. de Leitenburg, G. Dolcetti, A. Trovarelli, Catal. Today 114 (2006) 40.
[22] P. Palmisano, N. Russo, P. Fino, D. Fino, C. Badini, Appl. Catal. B 69 (2006) 85.
[23] T. Masui, K. Minami, K. Koyabu, N. Imanaka, Catal. Today 117 (2006) 187.
[24] E. Aneggi, J. Llorca, C. de Leitenburg, G. Dolcetti, A. Trovarelli, Appl. Catal. B 91 (2009) 489.
[25] M. Machida, Y. Murata, K. Kishikawa, D. Zhang, K. Ikeue, Chem. Mater. 20 (2008) 4489.
[26] K. Shimizu, H. Kawachi, A. Satsuma, Appl. Catal. B 96 (2010) 169.
[27] S.R. Seyedmonir, D.E. Strohmayer, G.J. Guskey, G.L. Geoffroy, M.A. Vannice, J. Catal. 93 (1985) 288.
[28] T. Kayama, K. Yamazaki, H. Shinjoh, J. Am. Chem. Soc. 132 (2010) 13154.
[29] F. Dong, A. Suda, T. Tanabe, Y. Nagai, H. Sobukawa, H. Shinjoh, M. Sugiura, C. Descorme, D. Duprez, Catal. Today 90 (2004) 223.
[30] F. Dong, A. Suda, T. Tanabe, Y. Nagai, H. Sobukawa, H. Shinjoh, M. Sugiura, C. Descorme, D. Duprez, Catal. Today 93-95 (2004) 827.
[31] X. Zang, K.J. Klabunde, Inorg. Chem. 31 (1992) 1706.
[32] X. Li, A. Vannice, J. Catal. 151 (1995) 87.
[33] L. Gang, B.G. Anderson, J. van Grondelle, R.A. van Santen, Appl. Catal. B 40 (2003) 101.
[34] C.T. Campbell, Surf. Sci. 157 (1985) 43.
[35] S.N. Trukhan, V.P. Ivanov, B.S. Bal'zhinimaev, Kinet. Catal. 38 (1997) 565.
[36] G.W. Busser, O. Hinrichsen, M. Muhler, Catal. Lett. 79 (2002) 49.
[37] M.J. Lippits, A.C. Gluhoi, B.E. Nieuwenhuys, Catal. Today 137 (2008) 446.
[38] B.S. Bal'zhinimaev, Kinet. Catal. 40 (1999) 795.
[39] A. Takahashi, N. Hamakawa, I. Nakamura, T. Fujitani, Appl. Catal. A 294 (2005) 34.
[40] G.I.N. Waterhouse, G.A. Bowmaker, J.B. Metson, Appl. Catal. A 265 (2004) 85.
[41] L. Kundakovic, M. Flytzani-Stephanopoulos, Appl. Catal. A 183 (1999) 35.
[42] J.C. Wu, P. Harriott, J. Catal. 39 (1975) 395.
[43] X.E. Verykios, F.P. Stein, R.W. Coughlin, J. Catal. 66 (1980) 368.
[44] C. Li, Y. Song, Y. Chen, Q. Xin, X. Han, W. Li, Stud. Surf. Sci. Catal. 112 (1997) 439.
[45] D. Duprez, Stud. Surf. Sci. Catal. 112 (1997) 13.
[46] D. Martin, D. Duprez, J. Phys. Chem. 100 (1996) 9429.